LETTERS
PUBLISHED ONLINE: 10 FEBRUARY 2013 | DOI: 10.1038/NGEO1723
nature geoscience

Estimated strength of the Atlantic overturning circulation during the last deglaciation

Stefan P. Ritz[1,2]*, Thomas F. Stocker[1,2], Joan O. Grimalt[3], Laurie Menviel[4] and Axel Timmermann[5]

The Atlantic meridional overturning circulation affects the latitudinal distribution of heat, and is a key component of the climate system. Proxy reconstructions, based on sedimentary $^{231}Pa/^{230}Th$ ratios and the difference between surface- and deep-water radiocarbon ages, indicate that during the last glacial period, the overturning circulation was reduced during millennial-scale periods of cooling[1–5]. However, much debate exists over the robustness of these proxies[6–8]. Here we combine proxy reconstructions of sea surface and air temperatures and a global climate model to quantitatively estimate changes in the strength of the Atlantic meridional overturning circulation during the last glacial period. We find that, relative to the Last Glacial Maximum, the overturning circulation was reduced by approximately 14 Sv during the cold Heinrich event 1. During the Younger Dryas cold event, the overturning circulation was reduced by approximately 12 Sv, relative to the preceding warm interval. These changes are consistent with qualitative estimates of the overturning circulation from sedimentary $^{231}Pa/^{230}Th$ ratios. In addition, we find that the strength of the overturning circulation during the Last Glacial Maximum and the Holocene epoch are indistinguishable within the uncertainty of the reconstruction.

The Atlantic meridional overturning circulation (AMOC) is an important feature of the Earth's climate system. It is characterized by northward-flowing water masses at the surface ocean, deep-water formation in the North Atlantic and southward-flowing water masses in the intermediate to deep ocean. This overturning cell is complemented by an underlying, generally weaker, reversed overturning cell that originates in the Southern Ocean. In the following, we use AMOC to refer only to the upper overturning cell. Owing to the large heat capacity of water, the northward-flowing near-surface waters contribute effectively to the heat transport from the tropics to the mid- and high latitudes and therefore affect the regional climate around the North Atlantic[9,10]. Hence, changes of the AMOC strength can substantially influence climate in the north, especially in Europe. The depth of the southward-flowing waters and the strength of the circulation have changed in the past. During the last glacial period, abrupt warming events of several degrees within a few decades followed by slower cooling were detected in Greenland ice cores[11]. As effects of the so-called Dansgaard–Oeschger events were found far beyond the Greenland ice sheet[12–14] with patterns reminiscent of varying inter-hemispheric heat distribution[15,16], they are believed to be the result of rapid changes of the AMOC strength[17]. Other examples of a reduction or even a complete shutdown of the AMOC are Heinrich stadial 1 from approximately 16.8 to 14.6 kyr before present (BP, before the year 1950 AD)[18], the Younger Dryas stadial from approximately 12.8 to 11.6 kyr BP (ref. 19) and the 8.2 kyr event[20].

In this study, we present a numerical reconstruction scheme to infer the past evolution of the AMOC strength on centennial to glacial–interglacial timescales. The scheme is based on earlier work[21] that proposes that ocean temperature anomalies at any location (i), T'^{i}_{oc}, can be approximated by a linear combination of anomalies of global mean air temperature (T'_{atm}), AMOC (Ψ'_{AMOC}) and Southern Ocean meridional overturning circulation (SOMOC) strength. The strength of the circulation is defined by the maximum of the meridional overturning stream function. In this study we focus on the surface Atlantic, where the effect of the SOMOC can be neglected[21]. Hence, we can linearly approximate the time evolution of the surface temperature pattern $T'^{i}_{oc}(t)$ as

$$T'^{i}_{oc}(t) = a^{i}_{Tatm} \cdot T'_{atm}(t) + a^{i}_{AMOC} \cdot \Psi'_{AMOC}(t) \quad (1)$$

The relationships between Atlantic sea surface temperature (SST), air temperature and AMOC are the result of ocean dynamics, and we determine coefficients (a^{i}_{Tatm} and a^{i}_{AMOC}) describing the postulated linear relationships using a global climate model, subject to a combination of forcings (see Methods). Global mean air temperature time series can be determined from air temperature reconstructions from Antarctic ice cores[22] and SST time series reconstructions are available from several marine sediment cores. Hence, equation (1) can be solved for Ψ'_{AMOC}. When several SST records are incorporated into the reconstruction, a least-squares solution can be calculated:

$$\Psi'_{AMOC}(t) = \sum_{i=1}^{n} \frac{w_i}{a^{i}_{AMOC}} [T'^{i}_{oc}(t) - a^{i}_{Tatm} T'_{atm}(t)] \quad (2)$$

where w_i is the weight of location i and is determined by the least-squares solver.

The simplicity of our assumption requires thorough testing of the reconstruction method. This is accomplished by hind-casting the AMOC strength of two model simulations from two independent climate models. In addition, the coefficients of the reconstruction scheme are calculated by two independent models (Fig. 1): by an ensemble of simulations performed with the Bern3D Earth System Model of intermediate complexity (hereafter B3D; Supplementary Fig. S2 and Table S3), and by a transient deglaciation simulation performed using the LOVECLIM

[1]Climate and Environmental Physics, Physics Institute, University of Bern, Sidlerstr. 5, 3012 Bern, Switzerland, [2]Oeschger Centre for Climate Change Research, University of Bern, 3012 Bern, Switzerland, [3]Department of Environmental Chemistry, Institute of Environmental Assessment and Water Research, Spanish Council for Scientific Research, 08034 Barcelona, Spain, [4]Climate Change Research Centre, Centre of Excellence, University of New South Wales, Sydney, New South Wales 2052, Australia, [5]IPRC, University of Hawaii, Honolulu, Hawaii 96822, USA. *e-mail: ritz@climate.unibe.ch.

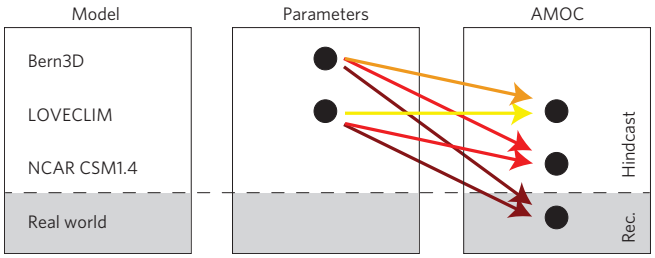

Figure 1 | Overview of the performed AMOC hindcasts and reconstructions. The colour of the arrows indicates the order of appearance within the paper (going from light to dark shading). The centre column indicates which models are used to calculate the coefficients of the reconstruction scheme. For example, coefficients determined from the Bern3D model are used to hindcast AMOC in LOVECLIM and NCAR models for verification with the directly simulated AMOC in these models, and to reconstruct AMOC from palaeoclimate records.

Earth System Model of intermediate complexity[23] (hereafter LVC; Supplementary Fig. S4 and Table S4). In both cases, a broad range of climate states is generated in response to various freshwater and CO_2 forcings that alter the AMOC, SST and global mean air temperature, respectively. Using the coefficients derived from the B3D and the LVC sensitivity experiments, AMOC hindcasts are calculated for the LVC simulation, and for a freshwater forcing simulation conducted with the National Center for Atmospheric Research (NCAR) CSM1.4 coupled atmosphere–ocean general circulation model[24] (hereafter CSM; Supplementary Information and Fig. S5).

For the AMOC hindcasts, we substitute the real world by one of the model simulations and reconstruct the AMOC evolution on the basis of our method using simulated SST time series from several Atlantic locations as well as global mean air temperature time series. The reconstructed AMOC evolution can then be compared to the temporal evolution of the true model AMOC. For both AMOC hindcasts, 14 model SST time series of the Atlantic Ocean are used (Supplementary Fig. S1). The locations of the time series correspond to locations where real SST reconstructions of the last deglaciation are available with an average resolution of at least 500 years (Supplementary Table S1). These SST records will be used later for the reconstruction of the deglacial AMOC variability.

As a first test, an AMOC hindcast of the LVC simulation is calculated, where the reconstruction scheme coefficients are also determined from the LVC simulation (Fig. 2a). The hindcast correlates well with the modelled AMOC ($R = 0.97$) and the relative standard deviation of $s_{rel} = 1.03$ is close to the optimum value of 1 (s_{rel} is defined as the standard deviation of the hindcast AMOC divided by the standard deviation of the modelled AMOC). The LVC hindcast is also successful when coefficients determined from the B3D simulations are used ($R = 0.97$, $s_{rel} = 0.85$; Fig. 2a). The largest discrepancy between hindcast and model AMOC appears during the Bølling between 15 and 14 kyr BP, where the AMOC peak of the model is not captured by the hindcast. The peak would be better captured if SSTs from the central North Atlantic (at approximately 50° N, 35° W) were incorporated into the hindcast (Supplementary Fig. S6). Unfortunately, at present there are no palaeo-SST reconstructions available from this region and hence we have not included this region in our analysis.

The weights that the least-squares solver assigns to the individual SST locations determines the relative contributions of the individual SST time series to the AMOC hindcast. The smaller the weight, the less sensitive the temperature at the particular

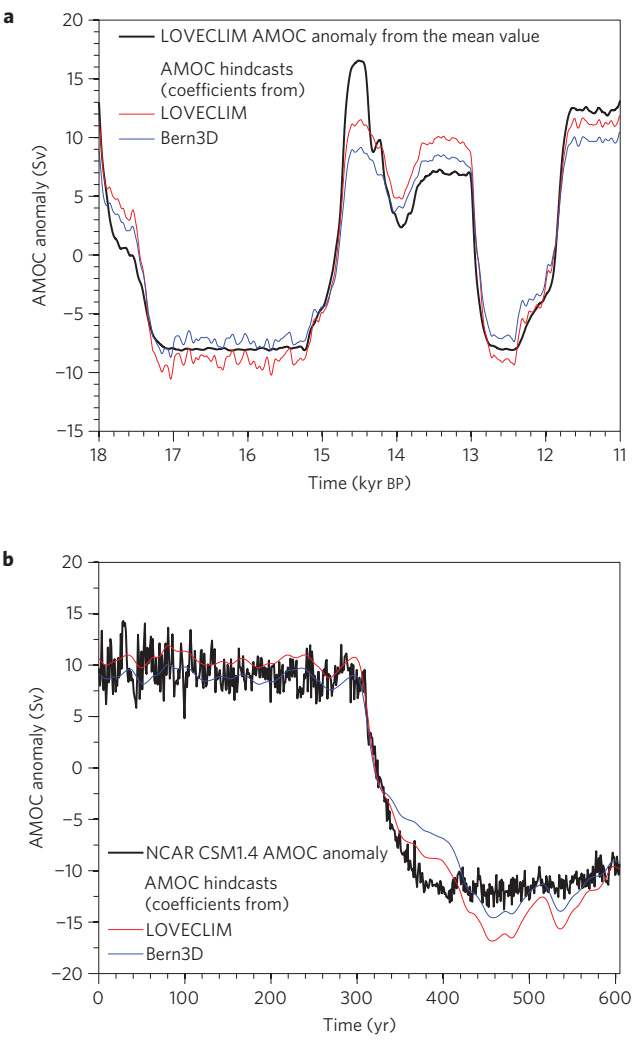

Figure 2 | AMOC hindcasts of two model simulations. The hindcast is given as anomalies from the time series mean value. **a**, Hindcast of the AMOC of a LOVECLIM deglaciation simulation[23] (Supplementary Fig. S4) using 14 Atlantic SST time series (Supplementary Fig. S1). Black line, LOVECLIM AMOC anomaly. Red line, AMOC hindcast calculated from coefficients determined by the LOVECLIM simulation. Blue line, hindcast from coefficients determined by Bern3D. The coefficients are given in Supplementary Tables S3 and S4. **b**, Hindcast of the AMOC of a freshwater forcing simulation[24] (Supplementary Fig. S5). Black line, NCAR CSM1.4 AMOC anomaly. Red line, AMOC hindcast calculated from coefficients determined by LOVECLIM. Blue line, hindcast from coefficients determined by Bern3D.

location is to changes of AMOC strength. The six northeastern Atlantic SST time series together have the largest influence on the hindcasts and account for a cumulative weight of about 90% (see Supplementary Table S5 for a list of the weights).

Next, the AMOC of the CSM model is hindcast (Fig. 2b). The atmospheric component of this model is considerably more complex than LVC. Again, both hindcasts calculated using LVC and B3D coefficients are very similar and compare well to the CSM model AMOC (for LVC coefficients: $R = 0.98$, $s_{rel} = 1.12$; for B3D coefficients: $R = 0.97$, $s_{rel} = 0.96$).

The hindcasts of the LVC deglaciation simulation and of the CSM freshwater forcing simulation emphasize the robustness of the AMOC reconstruction method. In the following, we apply the method to Atlantic SST reconstructions from marine sediment

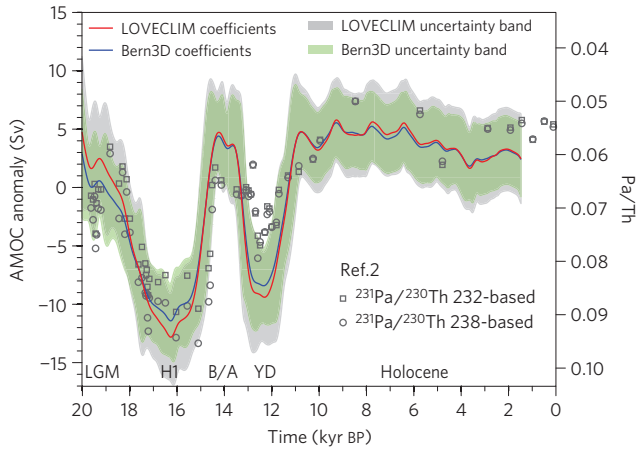

Figure 3 | Reconstruction of the AMOC of the last deglaciation. The reconstruction is given as anomalies from the time series mean value. For the reconstruction, 13 Atlantic SST time series are used (Supplementary Fig. S1 and Table S1) as well as global mean air temperature, which is determined from the Antarctic air temperature reconstruction from the EPICA Dome C Antarctic ice core[25] by applying a polar amplification factor and low-pass filtering the data to remove local- to hemispheric-scale variability. Blue line and green uncertainty band: reconstruction using the coefficients calculated from Bern3D. Red line and grey uncertainty band: reconstruction using the coefficients calculated from the LOVECLIM model. The uncertainty bands are determined by uncertainty propagation of the age-scale uncertainties of ±500 years, and the uncertainties that arise from the ocean and air temperature time series reconstructions. The uncertainty band of the reconstruction based on Bern3D coefficients additionally includes coefficient uncertainties. The reconstruction shows different AMOC regimes during the LGM, Heinrich stadial 1 (H1), the Bølling–Allerød (B/A), the Younger Dryas (YD) stadial and the Holocene. Dark grey symbols: qualitative AMOC reconstruction from sedimentary $^{231}Pa/^{230}Th$ (ref. 2).

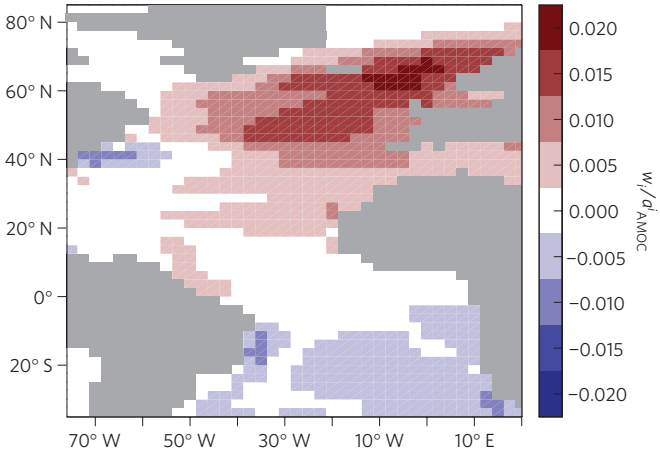

Figure 4 | Suitable locations of SST records for the AMOC reconstruction. An AMOC hindcast of the NCAR CSM1.4 simulation is calculated on the basis of SST time series of every LOVECLIM surface Atlantic model cell and by using reconstruction scheme coefficients determined from the LOVECLIM model. w_i/a^i_{AMOC} is the spatial fingerprint of the AMOC (equation (3)). It determines the influence of every location i on the AMOC hindcast. The larger the absolute values (the darker the colours), the larger the influence of the location on the AMOC hindcast.

cores to estimate the AMOC anomalies of the last deglaciation. One of the 14 SST records goes back only to 19 kyr BP. We do not use this record for the AMOC reconstruction to extend the reconstruction back to the Last Glacial Maximum (LGM). Owing to the small weight of this location, this has little impact on the result. The SST data are splined using a cutoff period of $\tau_{cut} = 1{,}000$ years. As there is no direct proxy for global mean air temperature, it is determined from the Antarctic air temperature reconstruction from the EPICA Dome C ice core[25] by low-pass filtering the data using a cutoff period of 10 kyr to remove local- to hemispheric-scale variability (such as the Antarctic Cold Reversal) and by applying a polar amplification factor of 2 that is determined from comprehensive global atmosphere–ocean general circulation models from the Paleoclimate Modelling Intercomparison Projects PMIP-1 and PMIP-2 (ref. 22).

Two AMOC reconstructions are presented: one using coefficients calculated from the B3D simulation, and one using coefficients calculated from the LVC simulation (Fig. 3). The 1σ-uncertainty band of the AMOC reconstruction follows from Gaussian uncertainty propagation of the individual uncertainties (Supplementary Information). These are the uncertainties of the SST reconstructions (Supplementary Table S1) and the air temperature reconstruction (±1.5 °C), the uncertainties of the age scales of the individual temperature reconstructions (±500 yr for the last deglaciation), and the uncertainties of the coefficients of the reconstruction scheme. The uncertainty band is calculated separately for the reconstruction using the B3D coefficients and for the reconstruction using the LVC coefficients.

The two reconstructions are very similar (Fig. 3). The AMOC during Heinrich stadial 1 (H1) is approximately 14 Sv weaker than during the LGM with a range of 5–23 Sv decrease. With a present-day AMOC strength of around 19 Sv ±5 Sv (ref. 26), this suggests a substantial slowdown of the AMOC during H1. The reconstruction also shows an AMOC slowdown during the Younger Dryas stadial by 12 Sv with a range of 5–22 Sv decrease in circulation compared with the Bølling–Allerød interstadial. The reconstruction is consistent with the AMOC reconstruction in ref. 2. However, our reconstruction suggests a stronger reduction of the AMOC during the Younger Dryas. Furthermore, the LGM-to-Holocene AMOC difference is less prominent in our reconstruction than in the $^{231}Pa/^{230}Th$ data.

We can use our method to determine locations for SST records that would be most effective for an AMOC reconstruction. Equation (2) can be rearranged to

$$\Psi'_{AMOC}(t) = \sum_{i=1}^{n} \frac{w_i}{a^i_{AMOC}} T'^{i}_{oc}(t) - \beta T'_{atm}(t) \qquad (3)$$

where $\beta = \sum_{i=1}^{n}(w_i a^i_{Tatm}/a^i_{AMOC})$, and w_i/a^i_{AMOC} is the spatial fingerprint of the AMOC. It determines the influence of every location (i) on the AMOC hindcast. To assess these fingerprints, we calculated an AMOC hindcast of the CSM simulation on the basis of SST time series of every LVC surface Atlantic model cell and by using reconstruction scheme coefficients determined from the LVC model (Fig. 4). Not surprisingly, the result is a bipolar seesaw pattern with the largest fingerprints in the northeast Atlantic.

Our AMOC reconstruction method can also be applied on longer timescales to reconstruct the AMOC over multiple glacial–interglacial cycles. However, a substantially larger age-scale uncertainty must be applied when radiocarbon dating is not available. Furthermore, changes of other large-scale circulations can potentially be reconstructed such as the SOMOC. In this case, deep ocean temperature time series reconstructions would be suitable candidates for the reconstruction. If deep ocean temperature reconstructions are included, then time lags between changes in air temperature, ocean circulation and ocean temperatures need to be allowed for in equation (1), that

is, $T'_{\mathrm{atm}}(t-\tau^i_{\mathrm{Tatm}})$ and $\Psi'_{\mathrm{SOMOC}}(t-\tau^i_{\mathrm{SOMOC}})$. Further, a possible occurrence of a North Pacific meridional overturning circulation cell during Heinrich stadials could be reconstructed[27]. However, both SOMOC and North Pacific meridional overturning circulation reconstructions would require further ocean temperature time series reconstructions at locations that are sensitive to these circulation changes.

Methods

Methodology. The reconstruction of the AMOC strength is based on the assumption that on centennial to glacial–interglacial timescales, SST anomalies (T'^i_{oc}) at any location in the Atlantic i can be approximated by a linear combination of global mean air temperature anomalies (T'_{atm}) and AMOC strength anomalies (Ψ'_{AMOC}):

$$T'^i_{\mathrm{oc}}(t) = a^i_{\mathrm{Tatm}} \cdot T'_{\mathrm{atm}}(t) + a^i_{\mathrm{AMOC}} \cdot \Psi'_{\mathrm{AMOC}}(t)$$

We define the AMOC strength as the maximum of the Atlantic meridional overturning stream function. Anomalies are defined as $T'^i_{\mathrm{oc}}(t) = T^i_{\mathrm{oc}}(t) - \overline{T}^i_{\mathrm{oc}}$, with $T^i_{\mathrm{oc}}(t)$ being the SST at time t and $\overline{T}^i_{\mathrm{oc}}$ being the temperature averaged over a period of time, and analogously for T'_{atm} and Ψ'_{AMOC}.

This approximation is supported by a recent study[28] in which a principal component analysis of globally distributed palaeo-records of temperature revealed that 61% of the climate variability of the last deglaciation can be explained by a globally near-uniform pattern that is strongly correlated to the atmospheric CO_2change (representing global mean T'_{atm}), and 11% can be explained by the bipolar seesaw pattern between the hemispheres[16] that resembles the millennial-scale variability of the AMOC.

In this reconstruction scheme we also assume that coupled climate models are able to provide a reasonable physical relationship between changes of AMOC, air temperatures and ocean temperatures. Accepting these assumptions, then the coefficients of the reconstruction scheme, a^i_{Tatm} and a^i_{AMOC}, can be diagnosed from a global coupled ocean–atmosphere climate model. Then with T'_{atm} time series reconstructions from ice cores and T'_{oc} time series reconstructions from marine sediment cores, equation (1) can be solved for Ψ'_{AMOC}.

A model simulation is performed where a broad range of climate states is produced by subjecting the model to various types of transient perturbation, for example, by adding and removing fresh water from the North Atlantic to alter the AMOC strength, and for example, by adding and removing CO_2 from the atmosphere to change air temperature. With this simulation we produce artificial climate reconstructions, that is purely model-based time series of T'^i_{oc}, T'_{atm} and Ψ'_{AMOC}. At the location of every SST reconstruction (i), a^i_{Tatm} and a^i_{AMOC} are determined by multiple linear regression of the simulated SST evolution to the reconstruction scheme using the simulated global mean air temperature as well as the simulated AMOC strength:

$$(T'^i_{\mathrm{oc}})^{\mathrm{fit}}(t) = a^i_{\mathrm{Tatm}} \cdot (T'_{\mathrm{atm}})^{\mathrm{model}}(t) + a^i_{\mathrm{AMOC}} \cdot (\Psi'_{\mathrm{AMOC}})^{\mathrm{model}}(t)$$

and minimizing $J = \sum_{t_{\mathrm{oc}}=t_0}^{t_{\mathrm{end}}} [(T'_{\mathrm{oc}})^{\mathrm{fit}}(t_{\mathrm{oc}}) - (T'_{\mathrm{oc}})^{\mathrm{model}}(t_{\mathrm{oc}})]^2$. This results in estimates of the coefficients a^i_{Tatm} and a^i_{AMOC} (see Supplementary Fig. S3 for examples). In this study, these coefficients are determined by an ensemble of 80 simulations performed with the B3D model, and by a deglaciation simulation using the LVC model[23] (Supplementary Information).

T'_{atm} is ideally global mean air temperature, because AMOC changes hardly affect global mean temperatures. Global mean T'_{atm} captures temperature changes induced by changes of greenhouse gases and surface albedo. Unfortunately, so far there is no direct palaeoclimate proxy of global mean air temperature. It is therefore determined from an Antarctic air temperature reconstruction as described in the main text. Alternatively to global mean air temperatures, Antarctic air temperatures could be used, because T'_{atm} does not necessarily need to be independent of variations in AMOC (Supplementary Fig. S7). It is important that in this case also Antarctic air temperatures are used for the determination of the coefficients of the reconstruction scheme. However, a prerequisite for this is that the polar amplification must be realistically represented in the model where the coefficients are determined. Furthermore, Antarctic air temperatures may additionally be influenced by quantities other than the AMOC, which can lead to a systematic bias of the AMOC reconstruction.

Solving equation (1) for Ψ'_{AMOC} is trivial if only one SST time series reconstruction is used. If more than one T'^i_{oc} reconstruction is available, a least-squares solution can be calculated:

$$\Psi'_{\mathrm{AMOC}}(t) = \sum_{i=1}^{n} \frac{w_i}{a^i_{\mathrm{AMOC}}} [T'^i_{\mathrm{oc}}(t) - a^i_{\mathrm{Tatm}} T'_{\mathrm{atm}}(t)]$$

where w_i is the weight of location i and is determined by the least-squares solver. Note that inaccurate coefficients a^i_{Tatm} may lead to a trend in Ψ'_{AMOC} in the case where T'^i_{oc} and T'_{atm} change simultaneously such as during a deglaciation. This is illustrated in a hindcast of the LVC deglaciation simulation where all a^i_{Tatm} are set to 0 K K^{-1} (Supplementary Fig. S8).

Reconstructions of sea surface and air temperatures are generally not equally spaced in time. Hence, the time series are splined using a cutoff period of τ_{cut} years[29]. τ_{cut} must be chosen appropriately depending on the resolution of the selected atmosphere and SST time series. A smaller τ_{cut} will result in a better-resolved Ψ'_{AMOC} reconstruction.

The sensitivity of SSTs to changes in Ψ'_{AMOC} depends on the location. Some locations are not, or only weakly sensitive to changes in Ψ'_{AMOC}. At these locations, a_{AMOC} is close to zero. This may lead to large uncertainties in the AMOC reconstruction, because in this case equation (2) approaches singularity. However, as long as the suite of T'^i_{oc} time series includes data at locations that are sensitive to circulation changes, the least-squares solution of the system of equations will assign very small weights to the time series that are only weakly sensitive to AMOC.

Data. SST and air temperature data used in the reconstruction (Supplementary Table S1) were obtained at http://www.pangaea.de, http://www.ncdc.noaa.gov/paleo, or by personal communication. See Supplementary Table S2 for specific links.

Received 2 November 2012; accepted 11 January 2013; published online 10 February 2013

References

1. Lynch-Stieglitz, J. *et al.* Atlantic meridional overturning circulation during the Last Glacial Maximum. *Science* **316,** 66–69 (2007).
2. McManus, J. F., Francois, R., Gherardi, J-M. & Keigwin, L. D. Collapse and rapid resumption of Atlantic meridional circulation linked to deglacial climate changes. *Nature* **428,** 834–837 (2004).
3. Gherardi, J. M. *et al.* Glacial–interglacial circulation changes inferred from Pa-231/Th-230 sedimentary record in the North Atlantic region. *Paleoceanography* **24,** PA2204 (2009).
4. Lippold, J. *et al.* Strength and geometry of the glacial Atlantic Meridional Overturning Circulation. *Nature Geosci.* **5,** 813–816 (2012).
5. Robinson, L. F. *et al.* Radiocarbon variability in the western North Atlantic during the last deglaciation. *Science* **310,** 1469–1473 (2005).
6. Scholten, J. C. *et al.* Advection and scavenging: Effects on ^{230}Th and ^{231}Pa distribution off Southwest Africa. *Earth Planet. Sci. Lett.* **271,** 159–169 (2008).
7. Keigwin, L. D. & Boyle, E. A. Did North Atlantic overturning halt 17,000 years ago? *Paleoceanography* **23,** PA1101 (2008).
8. Lippold, J. *et al.* Does sedimentary ^{231}Pa/^{230}Th from the Bermuda rise monitor past Atlantic meridional overturning circulation? *Geophys. Res. Lett.* **36,** L12601 (2009).
9. Ganachaud, A. & Wunsch, C. Improved estimates of global ocean circulation, heat transport and mixing from hydrographic data. *Nature* **408,** 453–456 (2000).
10. Trenberth, K. & Caron, J. M. Estimates of meridional atmosphere and ocean heat transports. *J. Clim.* **14,** 3433–3443 (2001).
11. NGRIP members. High-resolution record of Northern Hemisphere climate extending into the last interglacial period. *Nature* **431** 147–151 (2004).
12. Schulz, H., von Rad, U. & Erlenkeuser, H. Correlation between Arabian Sea and Greenland climate oscillations of the past 110,000 years. *Nature* **393,** 54–57 (1998).
13. Peterson, L. C., Haug, G. H., Hughen, K. A. & Röhl, U. Rapid changes in the hydrologic cycle of the tropical Atlantic during the last glacial. *Science* **290,** 1947–1951 (2000).
14. Wang, Y. J. *et al.* A high-resolution absolute-dated Late Pleistocene monsoon record from Hulu Cave, China. *Science* **294,** 2345–2348 (2001).
15. EPICA Community Members. One-to-one coupling of glacial climate variability in Greenland and Antarctica. *Nature* **444,** 195–198 (2006).
16. Stocker, T. F. & Johnson, S. J. A minimum thermodynamic model for the bipolar seesaw. *Paleoceanography* **18,** 1087 (2003).
17. Stocker, T. F. Past and future reorganizations in the climate system. *Quat. Sci. Rev.* **19,** 301–319 (2000).
18. Hemming, S. R. Heinrich events: Massive late Pleistocene detritus layers of the North Atlantic and their global climate imprint. *Rev. Geophys.* **42,** RG1005 (2004).
19. Broecker, W. S. Was the Younger Dryas triggered by a flood? *Science* **312,** 1146–1148 (2006).
20. Barber, D. C. *et al.* Forcing of the cold event of 8,200 years ago by catastrophic drainage of Laurentide lakes. *Nature* **400,** 344–348 (1999).
21. Ritz, S. P., Stocker, T. F. & Joos, F. A coupled dynamical ocean–energy balance atmosphere model for paleoclimate studies. *J. Clim.* **24,** 349–375 (2011).
22. Masson-Delmotte, V. *et al.* EPICA Dome C record of glacial and interglacial intensities. *Quat. Sci. Rev.* **29,** 113–128 (2010).
23. Menviel, L., Timmermann, A., Elison Timm, O. & Mouchet, A. Deconstructing the Last Glacial termination: The role of millennial and orbital-scale forcings. *Quat. Sci. Rev.* **30,** 1155–1172 (2011).

24. Bozbiyik, A., Steinacher, M., Joos, F., Stocker, T. F. & Menviel, L. Fingerprints of changes in the terrestrial carbon cycle in response to large reorganizations in ocean circulation. *Clim. Past* **7,** 319–338 (2011).
25. Jouzel, J. *et al.* Orbital and millennial Antarctic climate variability over the past 800,000 years. *Science* **317,** 793–796 (2007).
26. Rayner, D. *et al.* Monitoring the Atlantic meridional overturning circulation. *Deep Sea Res. II* **58,** 1744–1753 (2011).
27. Okazaki, Y. *et al.* Deepwater formation in the North Pacific during the last glacial termination. *Science* **329,** 200–204 (2010).
28. Shakun, J. D. & Carlson, A. E. A global perspective on Last Glacial Maximum to Holocene climate change. *Quat. Sci. Rev.* **29,** 1801–1816 (2010).
29. Enting, I. G. On the use of smoothing splines to filter CO_2 data. *J. Geophys. Res.* **92,** 10977–10984 (1987).

Acknowledgements

This study was financially supported by GRACCIE (CONSOLIDER-INGENIO 2010) and by the Swiss National Science Foundation. We thank F. Joos and C. Waelbroeck for fruitful discussions, M. Steinacher for providing the CSM data, and J. Jouzel for his help with the uncertainties of the ice core data.

Author contributions

S.P.R. and T.F.S. developed the method, A.T. contributed with ideas on method verification and AMOC fingerprinting, S.P.R. performed the B3D simulations, L.M. provided the LVC simulation, J.O.G. provided support of the sediment core data, and S.P.R. and T.F.S. wrote the manuscript. All authors discussed the results and provided input on the manuscript.

Additional information

Supplementary information is available in the online version of the paper. Reprints and permissions information is available online at www.nature.com/reprints. Correspondence and requests for materials should be addressed to S.P.R.

Competing financial interests

The authors declare no competing financial interests.